LBNL-39999
UC-405

ERNEST ORLANDO LAWRENCE
BERKELEY NATIONAL LABORATORY

Images as Embedding Maps and Minimal Surfaces: Movies, Color, and Volumetric Medical Images

R. Kimmel, N. Sochen, and R. Malladi
Computing Sciences Directorate
Mathematics Department

February 1997
To be presented at the
Computer Vision and Pattern Recognition Conference (CVPR'97),
San Juan, Puerto Rico,
June 17–19, 1997,
and to be published in
the Proceedings

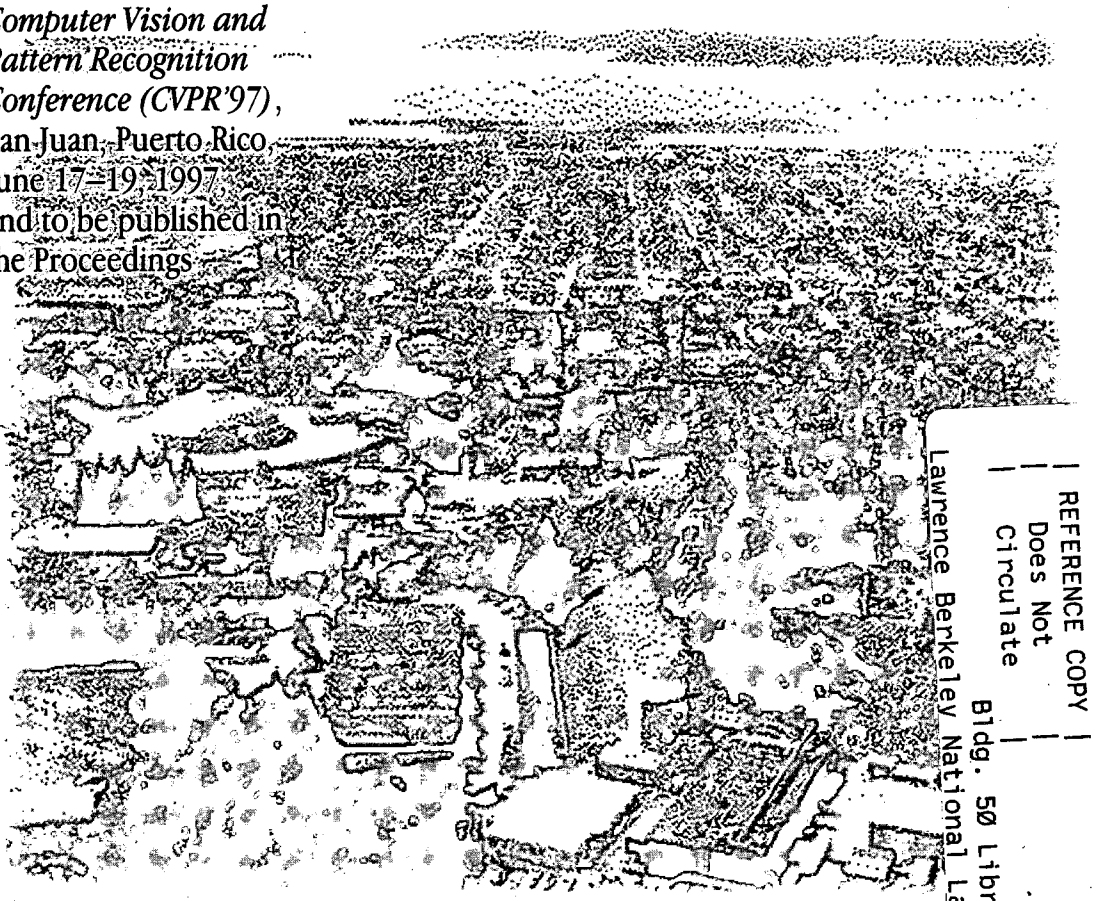

DISCLAIMER

LBNL-39999

IMAGES AS EMBEDDING MAPS AND MINIMAL SURFACES: MOVIES, COLOR, AND VOLUMETRIC MEDICAL IMAGES*

R. Kimmel
Mathematics Department
Lawrence Berkeley National Laboratory
University of California
Berkeley, CA 94720, USA

N. Sochen
Physics Department
Tel-Aviv University
Tel-Aviv 69978, Israel

R. Malladi
Mathematics Department
Lawrence Berkeley National Laboratory
University of California
Berkeley, CA 94720, USA

To be presented at:
Computer Vision and Pattern Recognition Conference
San Juan, Puerto Rico
June 17–19, 1997

*This work was supported in part by the Applied Mathematical Sciences subprogram of the Office of Energy Research, U.S. Department of Energy, under Contract DE-AC03-76SF00098, the Office of Naval Research under Grant N00014-96-1-0381, and the National Science Foundation under Grant PHY-90-21139.

Images as Embedding Maps and Minimal Surfaces: Movies, Color, and Volumetric Medical Images *

Ron Kimmel
Lawrence Berkeley National Laboratory
UC Berkeley, CA 94720

Nir Sochen
Raymond and Beverly Sackler Faculty of Exact Sciences
Tel-Aviv University, Israel

Ravi Malladi
Lawrence Berkeley National Laboratory
UC Berkeley, CA 94720

Abstract

A general geometrical framework for image processing is presented. We consider intensity images as surfaces in the $(\mathbf{x}, \mathbf{I})$ *space. The image is thereby a two dimensional surface in three dimensional space for gray level images. The new formulation unifies many classical schemes, algorithms, and measures via choices of parameters in a "master" geometrical measure. More important, it is a simple and efficient tool for the design of natural schemes for image enhancement, segmentation, and scale space. Here we give the basic motivation and apply the scheme to enhance images. We present the concept of an image as a surface in dimensions higher than the three dimensional intuitive space. This will help us handle movies, color, and volumetric medical images.*

1 Introduction

Motivated by [1, 21], we consider low level vision as an input to output process. For example, the most common input is a gray level image; namely a map from a two dimensional surface to a three dimensional space ($\mathbb{R}^3$). We have at each point of the xy coordinate plane an intensity $I(x, y)$. The $\mathbb{R}^3$ *space-feature* has Cartesian coordinates (x, y, I) where x and y are the *spatial* coordinates and I is the feature coordinate. The output of the low level process in most models consists of 1). A smoothed image from which reliable features can be extracted by local, and therefore differential operators. 2). A segmentation, that is, either a decomposition of the image domain into homogeneous regions with boundaries, or a set of boundary points – an "edge map".

The research on the low level vision process in the retina and the brain indicate the existence of layers serving as operators such that the information is processed locally in the layers and forwarded to the next layer with no interaction between distance layers. This means that the low level vision process can be described by a local differential operator. This process is called *scale space* where t is the scale (layer) parameter.

There are many definitions for scale spaces of images aiming to arrive at a coherent framework that unifies many assumptions. One such assumption is that *"only isophotes matter"*. We argue that this assumption, though leading to many interesting results in many cases, seems to fail in many other natural cases. Let us demonstrate it with a simple example: In Fig. 1 we see two images of a bright square on a darker background.

In fact, we notice that (see Fig. 2) in the second image the lower left corner of the 'bright square' is much darker than the upper right corner of the 'dark' background. Furthermore, even the upper right corner of the 'bright' square is darker than the upper right

*This work is supported in part by the Applied Mathematics Subprogram of the Office of Energy Research under DE-AC03-76SFOOO98, ONR grant under NOOO14-96-1-0381, and in part by the National Science Foundation under grant PHY-90-21139.

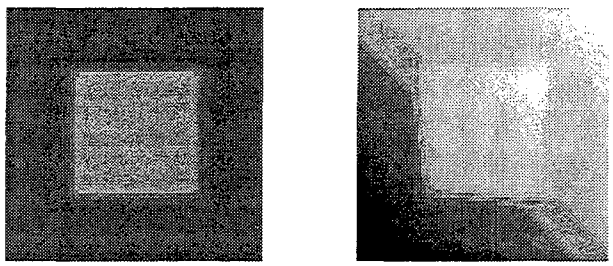

Figure 1: Two images of a bright square on dark background

corner of the 'dark' background. The boundary of the inner square in the left image is closely related to one of the isophotes of the gray level image in that image, as shown in the upper row of Fig. 2. In the second case, we added a smooth function - a tilted plane - to the first intensity function. This additional smooth function might be the result of non-uniform lighting conditions. It is obvious that in the second intensity image (the right image) the isophotes play only a minor role in the perception process of the image.

The importance of edges in scale space construction is obvious. Our view is consistent with the rest of the vision community in that boundaries between objects should survive as long as possible along the scale space, while homogeneous regions should be simplified and flattened in a more rapid way. On the other hand, we still want to preserve the geometry and mathematical integrity that results in some interesting non-linear 'scale spaces'. Another important question, for which there are only partial answers, is how to treat multi valued images. A color image is a good example since one actually talks about 3 images (Red, Green, Blue) that are composed into one. Should one treat such images as multi valued functions as proposed in [13]?

We attempt to answer some of the above questions by viewing images as *embedding maps*, that flow towards *minimal surfaces*. We consider two dimensions higher than most of the classical schemes, and instead of dealing with isophotes as planar curves we deal with the whole image as a surface. For example, a gray level image is no longer considered as a function but as a two dimensional surface in three dimensional space. In another example, we will show how to treat color images as a 2D surfaces in 5D: e.g. (x,y,R,G,B) space.

The remainder of this paper is organized as follows: In Section 2 we comment on the notions of metric and length needed for the definition of measure and the flow. We present in Sec. 3 our measure and a

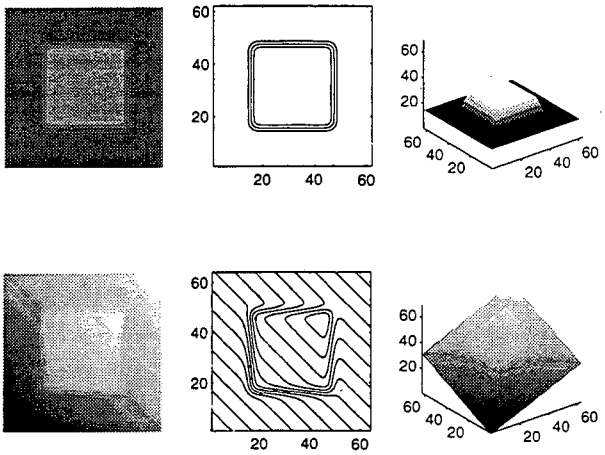

Figure 2: The two images from Fig. 1, their isophotes and the image as a surface in the (x, y, I) space.

choice of minimization that gives a generalized version of the mean curvature flow. Then, in Section 4 we introduce the flow itself that we have chosen to name *Beltrami flow*, and present a geometric interpretation in the simplest $3D$ case. Next, Section 5 presents the metric and the resulting flow for color images. The analysis of movies and volumetric medical images is presented in Sec. 7. We refer the interested reader to [28] for further details and examples including a new segmentation procedure motivated by [29].

2 The Metric

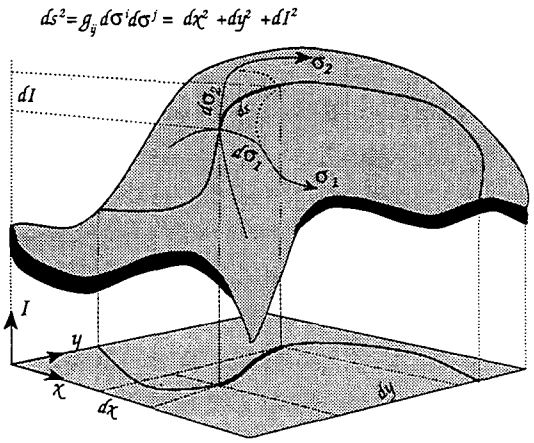

Figure 3: Length element of a surface curve ds.

The basic concept of Riemannian differential geometry is distance. Let us start with the impor-

tant example $X : \Sigma \rightarrow \mathbb{R}^3$. We denote the local coordinates on the two dimensional manifold Σ by (σ^1, σ^2). The map X is explicitly given by $(X^1(\sigma^1,\sigma^2), X^2(\sigma^1,\sigma^2), X^3(\sigma^1,\sigma^2))$. Since the local coordinates σ^i are curvilinear, and not orthogonal in general, the distance square between two close points on Σ, $p = (\sigma^1, \sigma^2)$ and $p + (d\sigma^1, d\sigma^2)$ is not $ds^2 = d\sigma_1^2 + d\sigma_2^2$. In fact, the squared distance is given by a positive definite symmetric bilinear form $g_{ij}(\sigma^1, \sigma^2)$ called the metric

$$\begin{aligned} ds^2 &= g_{\mu\nu} d\sigma^\mu d\sigma^\nu \\ &\equiv g_{11}(d\sigma^1)^2 + 2g_{12}d\sigma^1 d\sigma^2 + g_{22}(d\sigma^2)^2, \end{aligned} \quad (1)$$

where we used Einstein summation convention in the second equality; identical indices that appear one up and one down are summed over. We will denote the inverse of the metric by $g^{\mu\nu}$, so that $g^{\mu\nu}g_{\nu\gamma} = \delta^\mu_\gamma$, where δ^μ_γ is the Kronecker delta.

2.1 Induced metric

Let $X : \Sigma \rightarrow M$ be an embedding of Σ in M, where M is a Riemannian manifold with a metric $(g_{ij})_M$. We can use the knowledge of the metric on M and the map X to construct the metric on Σ. This procedure, is called the *pullback* and is given explicitly as follow:

$$(g_{\mu\nu})_\Sigma(\sigma^1,\sigma^2) = (g_{ij})_M(X(\sigma^1,\sigma^2))\partial_\mu X^i \partial_\nu X^j, \quad (2)$$

where $i, j = 1, ..., \dim M$ are being summed over, and in short we use $\partial_\mu X^i \equiv \frac{\partial X^i(\sigma^1,\sigma^2)}{\partial \sigma^\mu}$.

We will use the following simple and useful example that is often used in computer vision: Consider embedding of a surface described as a graph in $\mathbb{R}^3$,

$$X : (\sigma^1, \sigma^2) \rightarrow (\sigma^1, \sigma^2, I(\sigma^1, \sigma^2)). \quad (3)$$

Using Eq. (2) we get

$$(g_{\mu\nu}) = \begin{pmatrix} 1 + I_x^2 & I_x I_y \\ I_x I_y & 1 + I_y^2 \end{pmatrix} \quad (4)$$

where we used the identification $X^1 \equiv \sigma^1$ and $X^2 \equiv \sigma^2$ in the map X.

Actually we can understand this result in an intuitive way: Eq. (2) means that the distance measured on the surface by the local coordinates is equal to the distance measured in the embedding coordinates, see Fig. 3. Under the above identification, we can write

$$\begin{aligned} ds^2 &= dx^2 + dy^2 + dI^2 \\ &= dx^2 + dy^2 + (I_x dx + I_y dy)^2 \\ &= (1 + I_x^2)dx^2 + 2I_x I_y dx dy + (1 + I_y^2)dy^2. \end{aligned}$$

3 Polyakov Action and Harmonic Maps

In this section, we present a general framework for non-linear diffusion in computer vision. The equations will be derived by a minimization problem from an action functional. The functional in question depends on *both* the image manifold and the embedding space. Denote by (Σ, g) the image manifold and its metric and by (M, h) the space-feature manifold and its metric, then the map $X : \Sigma \rightarrow M$ has the following weight

$$S[X^i, g_{\mu\nu}, h_{ij}] = \int d^m\sigma \sqrt{g} g^{\mu\nu} \partial_\mu X^i \partial_\nu X^j h_{ij}(X), \quad (5)$$

where m is the dimension of Σ, g is the determinant of the image metric, $g^{\mu\nu}$ is the inverse of the image metric, the range of indices is $\mu, \nu = 1, \ldots, \dim\Sigma$, and $i, j = 1, \ldots, \dim M$, and h_{ij} is the metric of the embedding space. This functional, for $m = 2$, was first proposed by Polyakov [25] in the context of high energy physics, and the theory known as *string theory*.

Given the above functional, we have to choose the minimization. We may choose for example to minimize with respect to the embedding alone. In this case the metric $g_{\mu\nu}$ is treated as a parameter and may be fixed by hand. Another choice is to vary only with respect to the feature coordinates of the embedding space, or we may choose to vary the image metric as well. In [28] we show how different choices yield different flows. Some flows are recognized as existing methods like the heat flow, with passive coordinate transformation [16], the Perona-Malik flow [24], the geodesic active contours [5, 6, 17], the color flow [27, 8, 4], the mean-curvature flow [20] and its variants [14], and even a new invariant flow of images painted on surfaces [18]. Other choices are new and will be described below.

To gain some intuition about this functional, let us take the example of a surface embedded in $\mathbb{R}^3$ and treat both the metric $(g_{\mu\nu})$ and the spatial coordinates of the embedding space as free parameters, and fix them to

$$g = \begin{pmatrix} 1 & 0 \\ 0 & 1 \end{pmatrix} \quad , \quad x = \sigma^1 \quad , \quad y = \sigma^2. \quad (6)$$

From now on, we also fix the embedding space to Euclidean ($\mathbb{R}^3$ in the example at hand) with Cartesian coordinates (i.e. $h_{ij} = \delta_{ij}$). We refer the reader again to [28] for the general case. Then, up to a non-important constant, we get

$$S[I, g_{\mu\nu} = \delta_{\mu\nu}, h_{ij} = \delta_{ij}] = \int d^2\sigma |\nabla I|^2. \quad (7)$$

If we now minimize with respect to I, we will get the usual heat operator acting on I.

Using standard methods in variation calculus (see [28]), the Euler-Lagrange equations with respect to the embedding are:

$$-\frac{1}{2\sqrt{g}}h^{il}\frac{\delta S}{\delta X^l} = \frac{1}{\sqrt{g}}\partial_\mu(\sqrt{g}g^{\mu\nu}\partial_\nu X^i) \qquad (8)$$

Few remarks are in order. First notice that we used our freedom to multiply the Euler-Lagrange equations by a strictly positive function. Since $(g_{\mu\nu})$ is positive definite, $g \equiv \det(g_{\mu\nu}) > 0$ for all σ^μ. This factor is the simplest one that doesn't change the minimization solution while giving a reparametrization invariant expression. The operator that is acting on X^i is the natural generalization of the Laplacian from flat spaces to manifolds and is called *the second order differential parameter of Beltrami* [19], or for short *Beltrami operator*, and we will denote it by Δ_g.

For a surface Σ, embedded in 3 dimensional Euclidean space, we get a minimal surface as the solution to the minimization problem. In order to see that and to connect to the usual representation of the minimal surface equation, we notice that the solution of the minimization problem with respect to the metric is

$$g_{\mu\nu} = \partial_\mu X^i \partial_\nu X_i. \qquad (9)$$

On inspection, this equation is simply the induced metric on Σ. For the case of a surface embedded in $\mathbb{R}^3$ we calculated it explicitly in (see Eq. (4)). Plugging this induced metric in the first Euler-Lagrange, Eq. (8) we get the steepest decent flow

$$\vec{X}_t = H\vec{\mathcal{N}}, \qquad (10)$$

where H is the mean curvature, $\vec{\mathcal{N}}$ is the normal to the surface: [1]

$$\begin{aligned} H &= \frac{(1+I_x^2)I_{yy} - 2I_xI_yI_{xy} + (1+I_y^2)I_{xx}}{g^{\frac{3}{2}}}, \\ \vec{\mathcal{N}} &= \frac{1}{\sqrt{g}}(-I_y, -I_x, 1)^T, \end{aligned} \qquad (11)$$

and $g = 1 + I_x^2 + I_y^2$. We see that this choice gives us the mean curvature flow! This should not be a surprise, since the action functional for the above choice of metric $g_{\mu\nu}$ is

$$S = \int d^2\sigma\sqrt{g} = \int d^2\sigma\sqrt{\det(\partial_\mu X^i \partial_\nu X_i)},$$

which is the Euler functional that describes the area of the surface (also known in high energy physics as the Nambu action).

In general for any manifold Σ and M, the map $X : \Sigma \to M$ that minimizes the action S with respect to the embedding is called a **harmonic map**. The harmonic map is the natural generalization of the geodesic curve and the minimal surface to higher dimensional manifolds and for different embedding spaces.

The generalization to any manifold embedded with arbitrary co-dimension is given by using Eq. 8 for all the embedding coordinates and using the induced metric Eq. 9.

4 The Beltrami flow

In this section, we present a new and natural flow. The image is regarded as an embedding map $X : \Sigma \to \mathbb{R}^3$, where Σ is a two dimensional manifold, and the flow is natural in the sense that it minimizes the action functional with respect to I and (g_{ij}), while being reparametrization invariant. The coordinates X^1 and X^2 are parameters from this view point and are identified as above with σ^1 and σ^2 respectively. The result of the minimization is the Beltrami operator acting on I:

$$I_t = \Delta_g I \equiv \frac{1}{\sqrt{g}}\partial_\mu(\sqrt{g}g^{\mu\nu}\partial_\nu I) = H\vec{\mathcal{N}}_{\hat{I}}. \qquad (12)$$

where the metric is the induced one given in Eq. 2, and $\hat{I}$ is the unit vector in the I direction.

The geometrical meaning is obvious. Each point on the image surface moves with a velocity that depends on the mean curvature and the I component of the normal to the surface at that point. Since along the edges the normal to the surface lie almost entirely in the x-y plane, I hardly changes along the edges while the flow drives other regions of the image towards a minimal surface at a more rapid rate. Let us further explore the geometry of the flow in $3D$:

4.1 Geometric Flows Towards Minimal Surfaces

A minimal surface is the surface with the least area that satisfies given boundary conditions. It has nice geometrical properties, and is often used as a natural model of various physical phenomena, e.g. soap bubbles "Plateau's problem", in computer aided design, in architecture (structural design), and recently even for medical imaging [7]. Numerical schemes for the mean curvature flow, and the construction of minimal surfaces under constraints, has been the subject of considerable research [12, 10, 11, 9].

[1] Note also that some definitions of the mean curvature include a factor of 2 that we omit in our definition.

For constructing the mean curvature flow of a gray level image as a surface, we follow three steps:

(1). Given the surface $\mathcal{S}$ that evolves according to the geometric flow $\frac{\partial \mathcal{S}}{\partial t} = \vec{F}$, where $\vec{F}$ is an arbitrary smooth flow field. The geometric deformation of $\mathcal{S}$ may be equivalently written as $\frac{\partial \mathcal{S}}{\partial t} = \langle \vec{F}, \vec{\mathcal{N}} \rangle \vec{\mathcal{N}}$, where $\vec{\mathcal{N}}$ is the unit normal of the surface at each point, and $\langle \vec{F}, \vec{\mathcal{N}} \rangle$ is the inner product (the projection of $\vec{F}$ on $\vec{\mathcal{N}}$). The tangential component affects only the internal parameterization of the evolving surface and does not influence its geometric shape.

(2). The mean curvature flow is given by: $\frac{\partial \mathcal{S}}{\partial t} = H\vec{\mathcal{N}}$, where H is the mean curvature of $\mathcal{S}$ at every point. Let us now use the relation given in Step 1:

(3). Considering the image function $I(x, y)$, as a parameterized surface $\mathcal{S} = (x, y, I(x, y))$. We may write the mean curvature flow as: $\frac{\partial \mathcal{S}}{\partial t} = \frac{H}{\langle \vec{\mathcal{N}}, \vec{Z} \rangle} \vec{Z}$, for any smooth vector field $\vec{Z}$ defined on the surface. Especially, we may choose $\vec{Z}$ as the $\hat{I}$ direction, i.e. $\vec{Z} = (0, 0, 1)$. In this case

$$\frac{1}{\langle \vec{\mathcal{N}}, \vec{Z} \rangle} \cdot \vec{Z} = \sqrt{1 + I_x^2 + I_y^2} \cdot (0, 0, 1) = \sqrt{g}(0, 0, 1). \tag{13}$$

Fixing the (x, y) parameterization along the flow (i.e. using the fixed x, y plane as the natural parameterization), we have $\mathcal{S}_t = \frac{\partial}{\partial t}(x, y, I(x, y)) = (0, 0, I_t(x, y))$. Thus, for tracking the evolving surface, it is enough to evolve I via $\frac{\partial I}{\partial t} = H\sqrt{1 + I_x^2 + I_y^2}$, where the mean curvature H is given as a function of the image I, see Fig. 4, and Eq. (11).

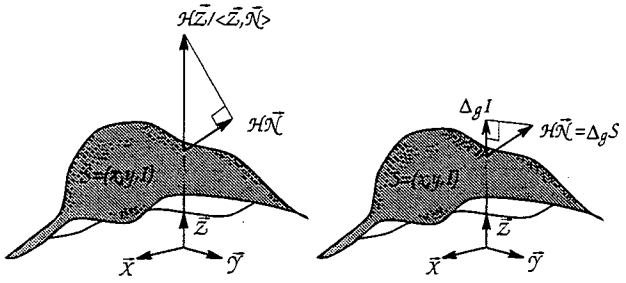

Figure 4: Left: Mean curvature flow. Right: Beltrami flow.

Substituting for H (see [10] for another derivation of H), we end up with the following evolution equation

$$I_t = \frac{(1 + I_y^2)I_{xx} - 2I_x I_y I_{xy} + (1 + I_x^2)I_{yy}}{1 + I_x^2 + I_y^2}, \tag{14}$$

with the image itself as initial condition $I(x, y, 0) = I(x, y)$. Using Beltrami second order operator Δ_g and the metric g, Eq. (14) may be read as $I_t = g\Delta_g I$. On the other hand, the Beltrami flow (selective mean curvature flow) $I_t = \Delta_g I$ is given explicitly for the simple 2D case as

$$I_t = \frac{(1 + I_y^2)I_{xx} - 2I_x I_y I_{xy} + (1 + I_x^2)I_{yy}}{(1 + I_x^2 + I_y^2)^2}, \tag{15}$$

see Fig. 4.

As an example, Fig. 5 compares the results of the Beltrami flow and the mean curvature flow both applied to a digital subtraction angiogram (DSA). It demonstrates the edge preserving property of the Beltrami flow relative to the mean curvature flow.

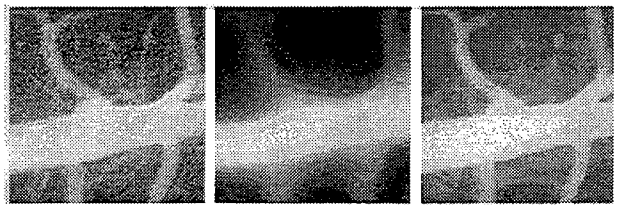

Figure 5: Left: Original medical image. Middle: Result of the mean curvature flow. Right: Result of the Beltrami flow.

We note again that some properties for the mean curvature flows that are relevant to some of our cases are studied by the PDE community, e.g. [2]. One important result, at least for the level set framework [23], in which the mapping is from $\mathbb{R}^m$ to $\mathbb{R}^{m+1}$ (embedding with codimension 1) is that embedding of evolving surfaces is preserved [15]. Roughly speaking, it means that surfaces can not cross as they evolve if they do not cross to begin with.

In [28] we show that large ratio between the gray level axis and one of the coordinate axis leads to potential surfaces via the heat equation [3, 22], while at small ratio we have the TV (total variation or L_1) [26]. We have thereby linked together many classical schemes via a selection of one parameter, that is, the image gray level scale with respect to its xy coordinates. This scale is determined arbitrarily anyhow in most of the current schemes.

5 Color

We generalize the Beltrami flow to the 5 dimensional space-feature needed in color images. The embedding space-feature space is taken to be Euclidean with Cartesian coordinate system. The image, thus,

is the map $f : \Sigma \rightarrow \mathbb{R}^5$ where Σ is a two dimensional manifold. Explicitly the map is

$$f = \left(X(\sigma^1,\sigma^2), Y(\sigma^1,\sigma^2), I^r(\sigma^1,\sigma^2), I^g(\sigma^1,\sigma^2), I^b(\sigma^1,\sigma^2)\right).$$

We note that there are obvious better selections to color space definition rather than the RGB flat space. Nevertheless, we get impressive results even from this oversimplified assumption.

We minimize our action (5) with respect to the metric and with respect to (I^r, I^g, I^b). For convenience we denote below (r, g, b) in general notation by i. Minimizing the metric gives, as usual, the induced metric which is given in this case as follows:

$$\begin{aligned} g_{11} &= 1 + (I^r_x)^2 + (I^g_x)^2 + (I^b_x)^2, \\ g_{12} &= I^r_x I^r_y + I^g_x I^g_y + I^b_x I^b_y, \\ g_{22} &= 1 + (I^r_y)^2 + (I^g_y)^2 + (I^b_y)^2, \\ g &= \det(g_{ij}) = g_{11}g_{22} - g_{12}^2. \end{aligned}$$

Note that this metric differs from the Di Zenzo metric [13] by the addition of 1 to g_{11} and g_{22}. The source of the difference is the map used to describe the image. Di Zenzo used $X : \mathbb{R}^2 \rightarrow \mathbb{R}^3$ while we use $X : \Sigma \rightarrow \mathbb{R}^5$.

The action functional under this choice of the metric is the Euler functional $S = \int d^2\sigma\sqrt{g}$. It is simply the area of the image surface. Minimization with respect to I^i gives the Beltrami flow

$$I^i_t = \frac{1}{\sqrt{g}}\partial_\mu(\sqrt{g}g^{\mu\nu}\partial_\nu I^i), \tag{16}$$

which is a flow towards a minimal surface that preserves edges.

For simple implementation of the Beltrami flow let us first compute the 6 matrices: I^i_x, I^i_y, and the following 6 matrices:

$$\begin{aligned} p^i &= g^{-1/2}(g_{22}I^i_x - g_{12}I^i_y), \\ q^i &= g^{-1/2}(g_{11}I^i_y - g_{12}I^i_x). \end{aligned} \tag{17}$$

Then the evolution is given by

$$I^i_t = g^{-1/2}\left(p^i_x + q^i_y\right). \tag{18}$$

In [28] we show that we can avoid the square root computations for this flow.

6 Beltrami Flow in Color Space

We now present some results of denoising color images using our model. Spatial derivatives are approximated using central differences and an explicit Euler step is employed to reach the solution. We represent

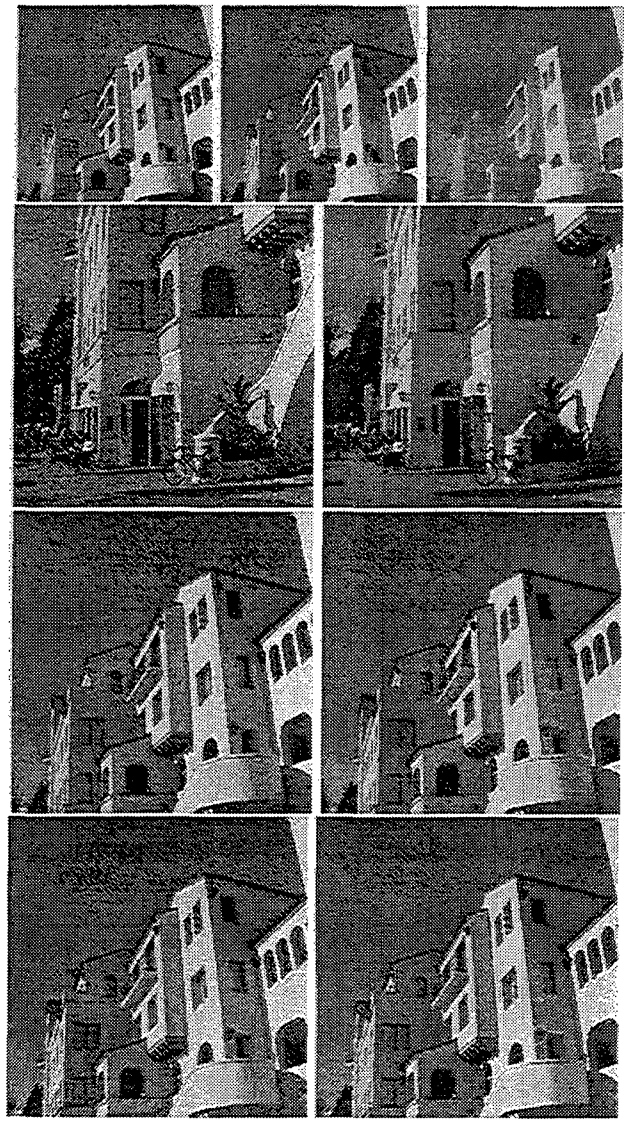

Figure 6: Color results

the image in the RGB space; however, other representations and different numerical schemes (as in [9]) are possible.

The results are presented in Fig. 6 as follows: In the first row of Fig. 6 the Beltrami flow is demonstrated to form an edge preserving scale space in color. Three images that correspond to different scales are presented left to right. Observe the way the fine geometric details disappear first, while sharp edges are preserved along the evolution.

The second row shows a color image corrupted with Gaussian noise. The reconstruction result by applying Beltrami flow is also shown on the right. Iteration has been manually stopped to produce the result. Constraints similar to [4] can be added; see [28] for details.

Finally, third and fourth rows of the figure present the result of applying present the result of applying the Beltrami flow to reconstruct a color image with noise artifacts introduced first by wavelet lossy compression and then by JPEG lossy compression. The left pair depicts the corrupted image and the right pair is the result of reconstructing it with the Beltrami flow.

7 Movies and Volumetric Medical Images

Traditionally, MRI volumetric data is referred to as 3D medical image. Following our framework, a more appropriate definition is of a 3D surface in 4D (x, y, z, I). In a very similar manner we will consider gray level movies as a 3D surfaces in 4D, where all we need to do is the mental exercise of replacing z of the volumetric medical images by the sequence (time) axis. In Fig. 7, the first row shows images at different z locations and the second row shows the corresponding denoised images, the third image in both sequences is magnified showing the selective smoothing effect in this case. This is a relatively simple case, since now we have co-dimension equal to one.

The induced metric in this case is given by

$$(g_{ij}) = \begin{pmatrix} 1+I_x^2 & I_xI_y & I_xI_z \\ I_xI_y & 1+I_y^2 & I_yI_z \\ I_xI_z & I_yI_z & 1+I_z^2 \end{pmatrix}, \qquad (19)$$

and the Beltrami flow is now:

$$\begin{aligned} I_t \;=\; g^{-2}\,(\;& I_{zz}(1+I_x^2+I_y^2)+I_{yy}(1+I_z^2+I_x^2) \\ & +I_{xx}(1+I_y^2+I_z^2)-2I_xI_yI_{xy} \\ & -2I_yI_zI_{yz}-2I_zI_xI_{zx}) \end{aligned} \qquad (20)$$

where $g = 1 + I_x^2 + I_y^2 + I_z^2$.

8 Concluding Remarks

Inventing a perceptually good segmentation process, and formulating a meaningful scale space for images is not an easy task, and is actually what low level vision research is about. Here we tried to address these questions and to come up with a new framework that unifies many previous results and introduces new procedures. There are still many open questions to be asked, like what is the right aspect ratio between the intensity and the image plane? Or in a more general sense, what is the 'right' embedding space h_{ij}?

The question of what is the 'right norm' when dealing with images is indeed not trivial, and the right answer probably depends on the application. For example, the answer for the 'right' color metric h_{ij} is the consequence of empirical results, experimental data, and the application. Here we covered some of the gaps between the two classical norms (L_1-TV and the L_2) in a geometrical way and proposed a new approach to deal with multi dimensional images. We used recent results from high energy physics that yield promising algorithms for enhancement, segmentation and scale space.

References

[1] L Alvarez and J M Morel. Morphological approach to multiscale analysis: From principles to equations. In B M ter Haar Romeny, editor, *Geometric-Driven Diffusion in Computer Vision.* Kluwer Academic Publishers, The Netherlands, 1994.

[2] L Ambrosio and H M Soner. Level set approach to mean curvature flow in arbitrary codimension. *J. of Diff. Geom.*, 43:693–737, 1996.

[3] A Blake and A Zisserman. *Visual Reconstruction.* MIT Press, Cambridge, Massachusetts, 1987.

[4] P Blomgren and T F Chan. Color TV: Total variation methods for restoration of vector valued images. cam TR, UCLA, 1996.

[5] V Caselles, R Kimmel, and G Sapiro. Geodesic active contours. In *Proceedings ICCV'95*, pages 694–699, Boston, Massachusetts, June 1995.

[6] V Caselles, R Kimmel, and G Sapiro. Geodesic active contours. *IJCV*, to appear, 1995.

[7] V Caselles, R Kimmel, G Sapiro, and C Sbert. Minimal surfaces: A geometric three dimensional segmentation approach. *Numerische Mathematik*, to appear, 1996.

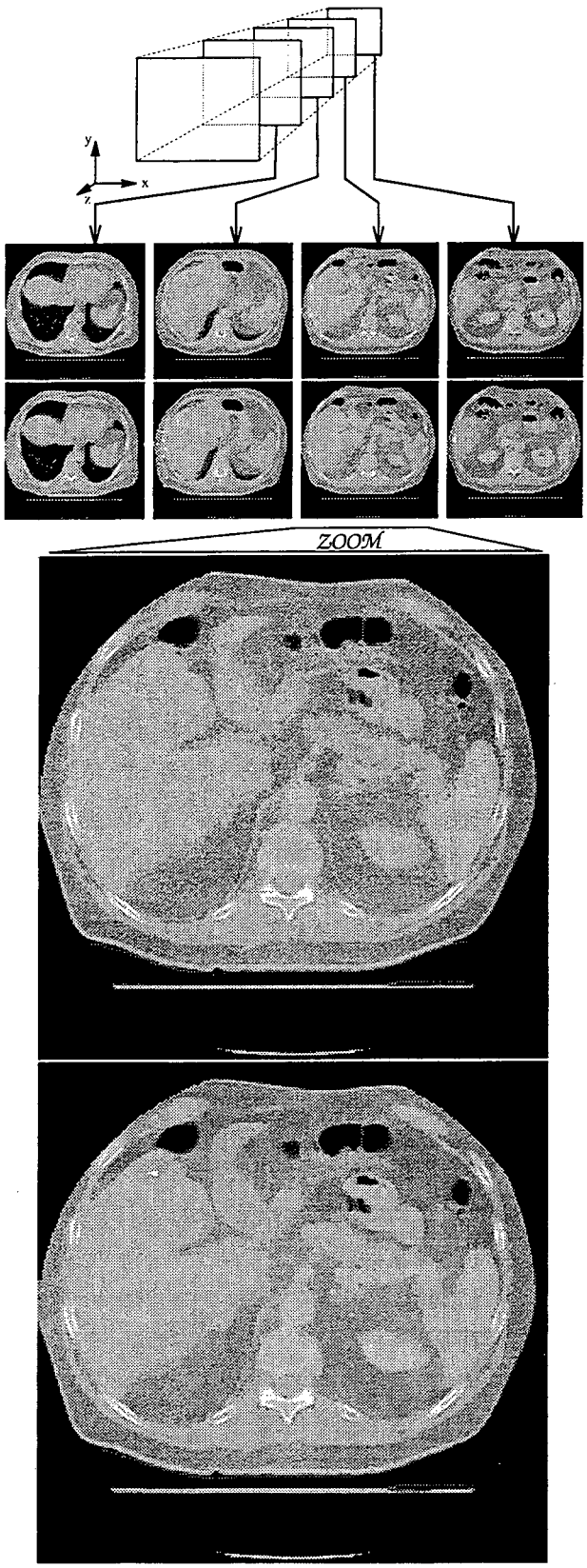

Figure 7: Movie or volumetric data; see text.

[8] A Chambolle. Partial differential equations and image processing. In *Proceedings IEEE ICIP*, Austin, Texas, November 1994.

[9] T F Chan, G H Golub, and P Mulet. A nonlinear primal-dual method for total variation-based image restoration. *Presented at AMS/SIAM workshop on Linear and Nonlinear CG methods*, July 1995.

[10] D L Chopp. Computing minimal surfaces via level set curvature flow. *J. of Computational Physics*, 106(1):77–91, May 1993.

[11] D L Chopp and J A Sethian. Flow under curvature: Singularity formation, minimal surfaces, and geodesics. *Jour. Exper. Math.*, 2(4):235–255, 1993.

[12] P Concus. Numerical solution of the minimal surface equation. *Mathematics of Computation*, 21:340–350, 1967.

[13] S Di Zenzo. A note on the gradient of a multi image. *Computer Vision, Graphics, and Image Processing*, 33:116–125, 1986.

[14] A I El-Fallah, G E Ford, V R Algazi, and R R Estes. The invariance of edges and corners under mean curvature diffusions of images. In *Processing III SPIE*, volume 2421, pages 2–14, 1994.

[15] L C Evans and J Spruck. Motion of level sets by mean curvature, I. *J. Diff. Geom.*, 33, 1991.

[16] L M J Florack, A H Salden, , B M ter Haar Romeny, J J Koendrink, and M A Viergever. Nonlinear scale-space. In B M ter Haar Romeny, editor, *Geometric–Driven Diffusion in Computer Vision*. Kluwer Academic Publishers, The Netherlands, 1994.

[17] S Kichenassamy, A Kumar, P Olver, A Tannenbaum, and A Yezzi. Gradient flows and geometric active contour models. In *Proceedings ICCV'95*, Boston, Massachusetts, June 1995.

[18] R Kimmel. Intrinsic scale space for images on surfaces: The geodesic curvature flow. LBNL Report LBNL 39172, LBNL UC Berkeley, CA 94720, August 1996.

[19] E Kreyszing. *Differential Geometry*. Dover Publications, Inc., New York, 1991.

[20] R Malladi and J A Sethian. Image processing: Flows under min/max curvature and mean curvature. *Graphical Models and Image Processing*, 58(2):127–141, March 1996.

[21] D Marr. *Vision*. Freeman, San Francisco, 1982.

[22] D Mumford and J Shah. Boundary detection by minimizing functionals. In *Proceedings of CVPR, Computer Vision and Pattern Recognition*, San Francisco, 1985.

[23] S J Osher and J A Sethian. Fronts propagating with curvature dependent speed: Algorithms based on Hamilton-Jacobi formulations. *J. of Comp. Phys.*, 79:12–49, 1988.

[24] P Perona and J Malik. Scale-space and edge detection using anisotropic diffusion. *IEEE-PAMI*, 12:629–639, 1990.

[25] A M Polyakov. *Physics Letters*, 103B:207, 1981.

[26] L Rudin, S Osher, and E Fatemi. Nonlinear total variation based noise removal algorithms. *Physica D*, 60:259–268, 1992.

[27] G Sapiro and D Ringach. Anisotropic diffusion of multivalued images. In *12th Int. Conf. on Analysis and Optimization of Systems: Images, Wavelets and PDE'S*, Paris, June 1996. Springer Verlag.

[28] N Sochen, R Kimmel, and R Malladi. From high energy physics to low level vision. Report LBNL 39243, LBNL, UC Berkeley, CA 94720, August 1996; submitted to *IEEE Trans. IP*.

[29] S D Yanowitz and A M Bruckstein. A new method for image segmentation. *Computer Vision, Graphics, and Image Processing*, 46:82–95, 1989.

Ernest Orlando Lawrence Berkeley National Laboratory
One Cyclotron Road | Berkeley, California 94720

Prepared for the U.S. Department of Energy under Contract No. DE-AC03-76SF00098